

Symplectic-Amoeba formulation of the non-Bloch band theory for one-dimensional two-band systems

Shin Kaneshiro^{1,*} and Robert Peters¹

¹*Department of Physics, Kyoto University, Kyoto 606-8502, Japan*

(Dated: February 26, 2025)

The non-Hermitian skin effect is a topological phenomenon, resulting in the condensation of bulk modes near the boundaries. Due to the localization of bulk modes at the edges, boundary effects remain significant even in the thermodynamic limit. This makes conventional Bloch band theory inapplicable and hinders the accurate computation of the spectrum. The Amoeba formulation addresses this problem by determining the potential from which the spectrum can be derived using the generalized Szegő's limit theorem, reducing the problem to an optimization of the Ronkin function. While this theory provides novel insights into non-Hermitian physics, challenges arise from the multiband nature and symmetry-protected degeneracies, even in one-dimensional cases. In this work, we investigate one-dimensional two-band class AII[†] systems, where Kramers pairs invalidate the conventional Amoeba formalism. We find that these challenges can be overcome by optimizing the band-resolved Ronkin functions, which is achieved by extrapolating the total Ronkin function. Finally, we propose a generalized Szegő's limit theorem for class AII[†] and numerically demonstrate that our approach correctly computes the potential and localization length.

I. INTRODUCTION

Non-Hermitian matrices are ubiquitous in a wide variety of physical systems, from classical wave dynamics to open quantum systems [1–3]. These matrices naturally describe non-conservative dynamics induced by the dissipation and the energy exchange in real systems. The presence of non-Hermiticity profoundly affects system properties, often leading to singular spectral structures with unique eigenstate distributions. A particularly striking consequence of non-Hermiticity is the Non-Hermitian Skin Effect (NHSE) [4–29]. This phenomenon, characterized by a point-gap spectral structure, arises from the interplay between non-Hermiticity and topology, which does not have a counterpart in Hermitian systems.

The NHSE fundamentally modifies the system's response to boundary conditions, resulting in exponentially localized bulk modes and a breakdown of conventional Bloch band theory. As a result, the eigenvalues and eigenstates under open boundary conditions (OBC) significantly deviate from those under periodic boundary conditions (PBC).

Complex wavenumbers with non-zero imaginary parts have been introduced to overcome this limitation, leading to a modified Bloch band theory. These generalizations are known as the non-Bloch band theory, which has established the concept of the generalized Brillouin zone [4, 6]. This non-Bloch band theory has achieved remarkable success in one-dimensional systems, including symmetry-protected cases [30], providing a comprehensive framework for understanding non-Hermitian one-dimensional systems [16, 31–51].

In contrast, attempts to extend the non-Bloch band

theory to higher dimensions have proved challenging [52–57]. While boundaries in one-dimensional systems are inherently simple, those in two or higher dimensions exhibit far more complex geometries. In this context, the recently proposed Amoeba theory has significantly advanced the field [58–62]. The Amoeba formulation defines the "electrical" potential of the spectrum, making it possible to access the density of states (DOS) under OBC for single-band class A systems in arbitrary dimensions. In particular, the generalized Szegő's limit theorem reduces the potential computation to an optimization of the Ronkin function. Furthermore, as the Ronkin function takes the inverse localization length as an argument, the solution to this optimization problem returns the correct localization length.

While the Amoeba formulation provides a powerful framework for developing the non-Bloch band theory of one-band systems, generalizing it to multiband systems remains challenging. In particular, degeneracies arising from the transpose-type time-reversal symmetry (TRS[†]) impose constraints on the Ronkin function [59], which obstruct both the optimization problem and the application of the generalized Szegő's limit theorem. These constraints are especially significant in symplectic classes, where TRS[†] leads to Kramer's degeneracies, further complicating the Amoeba formulation. Consequently, even for one-dimensional systems, the Amoeba formulation fails to apply to symplectic classes.

Here, we partially overcome this limitation by generalizing the Amoeba formulation to the one-dimensional two-band class AII[†]. Separating the Ronkin function into its band-resolved parts, which are related by the TRS[†] operation, we show that we can optimize these band-resolved Ronkin functions by extrapolating the total Ronkin function. This extrapolation is easily calculated by the Legendre transformation of the total Ronkin function and leads to a generalized Szegő's limit theorem for class AII[†] in one dimension.

* kaneshiro.shin.88a@st.kyoto-u.ac.jp

The rest of this paper is organized as follows: In Sec. II, we introduce our notation and briefly review the non-Bloch band theory and the Amoeba formulation in one-dimensional class A systems. In Sec. III, we propose the generalized Szegő's limit theorem for one-dimensional two-band class AIII[†] systems using the band-decomposition. In Sec. IV, we numerically verify our methods and theorems. Sec. V summarizes and concludes this paper. Furthermore, in Appendix A, we illustrate the dependency of the band-resolved Ronkin functions on branch cuts utilizing the energy band branches.

II. OBC BAND STRUCTURE FOR CLASS A SYSTEMS

This section introduces the notation and briefly reviews the non-Bloch band theory [4, 6, 7] and the Amoeba formulation [58] in class A systems.

A. Notations

We consider a one-dimensional lattice of length N with M states at each site. For simplicity, we set the lattice constant to unity. The OBC Hamiltonian $\hat{\mathcal{H}}$ is generally expressed as

$$\hat{\mathcal{H}} = \sum_{x,y=1}^N \sum_{a,b=1}^M \hat{c}_{x,a}^\dagger H_{xa,yb}^{(N)} \hat{c}_{y,b} \quad (1)$$

where $\hat{c}_{x,a}$, ($\hat{c}_{x,a}^\dagger$) annihilates (creates) a particle at site x in state a . Due to the periodicity of the lattice, the hopping amplitudes $H_{xa,yb}$ depend only on the relative distance between different sites and form a Block Toeplitz matrix $H^{(N)}$: $H_{xa,yb}^{(N)} = H_{x-y,ab}$. The Fourier transformation of these matrix elements yields the Bloch Hamiltonian,

$$h_{B,ab}(k) = \sum_{n=-p}^p H_{n,ab} e^{ikn}, \quad (2)$$

where the parameter p is the largest hopping distance.

In the absence of the NHSE, the spectrum of $H^{(N)}$ (OBC spectrum) is correctly approximated by the spectrum of $h_B(k)$ (PBC spectrum) except for $\mathcal{O}(1)$ edge modes, since the eigenstates are delocalized and approximated with plane waves with wavenumber k . On the other hand, if the NHSE occurs, a large number ($\mathcal{O}(N)$) OBC eigenstates become exponentially localized, and complex-valued wavenumbers emerge. To take into account such complex-valued wavenumbers, the non-Bloch Hamiltonian is defined through an analytic continuation of the Bloch Hamiltonian to $h_B(k - i\mu)$, where μ is the inverse localization length. In the following discussion, we denote the non-Bloch Hamiltonian as

$$h_{\text{nB}}(\beta) = h_B(-i \log \beta), \quad (3)$$

where $\beta = e^{\mu+ik}$. In this β representation, the non-Bloch Hamiltonian becomes a matrix-valued Laurent polynomial.

B. Non-Bloch band theory

The non-Bloch band theory determines the OBC band structure through a bivariate polynomial called the characteristic polynomial:

$$\text{ChP}(E, \beta) = \det[E - h_{\text{nB}}(\beta)]. \quad (4)$$

This polynomial establishes the relation between complex-valued wavenumbers β and energies E and generalizes the Bloch band theory.

The characteristic polynomial can be factorized in two complementary ways:

$$\begin{aligned} \text{ChP}(E, \beta) &= C_E \beta^{-Mp} \prod_{j=1}^{2Mp} (\beta - \beta_j(E)) \\ &= \prod_{\sigma=1}^M (E - E_\sigma(\beta)) \end{aligned} \quad (5)$$

where C_E is a β -independent constant. We assume that the β -roots, β_j , are ordered by their moduli: $|\beta_i(E)| \leq |\beta_j(E)|$ for $i \leq j$. Then, the E -roots, $E_\sigma(\beta)$, provide the energy band branches (EBB) [63]. For a model described by a rank- M matrix $h(\beta)$, there are M EBBs.

There are several β values associated with a given E through the characteristic polynomial. It has been found that for OBC, only a few $\beta_j(E)$ contribute to the OBC wave function. The concept of GBZ emerges from collecting these β values. In class A systems, the GBZ for band σ is characterized as:

$$\text{GBZ}_\sigma = \{\beta \in \mathbb{C}; |\beta_{Mp} \circ E_\sigma(\beta)| = |\beta_{Mp+1} \circ E_\sigma(\beta)|\}, \quad (6)$$

where \circ denotes a function composition [4, 6, 7]. The spectrum of band σ is then obtained by mapping the GBZ_σ through E_σ .

While the non-Bloch band formulation is applicable to multiband systems, generalizations to higher-dimensional systems are non-trivial since conditions analogous to Eq. (6) have not yet been established in higher-dimensional systems.

C. Amoeba formulation

The Amoeba formulation determines the OBC band structure through the OBC DOS and its potential. The OBC DOS on the complex-energy plane is defined using the Dirac's delta function as

$$\rho(E) = \lim_{N \rightarrow \infty} \frac{1}{N} \text{Tr} \delta(E - H^{(N)}). \quad (7)$$

This DOS is intimately connected to the OBC spectral potential $\phi(E)$ which satisfies the Laplace equation

$$\rho(E) = \frac{1}{2\pi} \Delta \phi(E), \quad (8)$$

where $\Delta = \partial^2/\partial(\text{Re } E)^2 + \partial^2/\partial(\text{Im } E)^2$. Since the complex-energy plane is two-dimensional, the potential can be rewritten as

$$\phi(E) = \lim_{N \rightarrow \infty} \frac{1}{N} \text{Tr} \ln |E - H^{(N)}|. \quad (9)$$

While the direct calculation of this potential requires the determinant of a huge matrix, it can be efficiently computed using the non-Bloch Hamiltonian under certain conditions.

In one-band class A systems, the spectral potential is given by Szegő's limit theorem [64],

$$\phi(E) = \int_{\ln|\beta|=0} \frac{d\beta}{2\pi i \beta} \ln |\text{ChP}(\beta, E)|, \quad (10)$$

for topologically trivial E , detected by a zero-winding number $W(E) = 0$, defined as

$$W(E) = \int_0^{2\pi} \frac{dk}{2\pi} \partial_k \ln \det[E - h_B(k)]. \quad (11)$$

This theorem states that the PBC spectral potential can be used for the OBC potential for trivial E .

Szegő's limit theorem is invalid for topologically non-trivial E , though a generalization is proposed in [58]. According to this conjecture, the potential $\phi(E)$ in one-dimensional single-band systems ($M = 1$) is given by a test potential $\Phi(E)$, which is determined through the following optimization problem:

$$\Phi(E) = \min_{\mu} R_E(\mu), \quad (12)$$

where R_E is the Ronkin function defined as

$$R_E(\mu) = \oint_{\ln|\beta|=\mu} \frac{d\beta}{2\pi i \beta} \ln |\text{ChP}(E, \beta)|. \quad (13)$$

The integration in Eq. (13) can be rewritten in terms of β using Eq. (5):

$$\begin{aligned} R_E(\mu) &= \ln |C_E| - p \oint_{\ln|\beta|=\mu} \frac{d\beta}{2\pi i \beta} \ln |\beta| \\ &+ \sum_{j=1}^{2p} \oint_{\ln|\beta|=\mu} \frac{d\beta}{2\pi i \beta} \ln |\beta - \beta_j(E)|. \end{aligned} \quad (14)$$

This representation indicates that the Ronkin function is determined by the pole and the roots of the characteristic equation enclosed by the circle $|\beta| = e^\mu$ [60]:

$$\begin{aligned} R_E(\mu) &= \ln |C_E| - p\mu \\ &+ \sum_{j=1}^{2p} \mu_j + \sum_{j=1}^{2p} (\mu - \mu_j) \cdot \theta(\mu - \mu_j), \end{aligned} \quad (15)$$

where $\mu_j = \ln |\beta_j(E)|$ and $\theta(x)$ is the step function, which takes the value 1 for $x \geq 0$ and 0 for $x < 0$. Thus, the Ronkin function is a convex and piece-wise linear function, and its derivative is quantized to integer values in one-dimensional systems.

Using this representation, we can expand the Ronkin function around its minimum as

$$R_E(\mu) = a + \begin{cases} -(\mu - \mu_p) & \mu_{p-1} \leq \mu \leq \mu_p \\ 0 & \mu_p \leq \mu \leq \mu_{p+1} \\ \mu - \mu_{p+1} & \mu_{p+1} \leq \mu \leq \mu_{p+2} \end{cases}, \quad (16)$$

where a is obtained by

$$a = \ln |C_E| + \sum_{j=p+1}^{2p} \mu_j. \quad (17)$$

In the Amoeba formulation, the absence of an intermediate region where the Ronkin function is constant indicates that E lies within the spectrum, and the μ^* , which minimizes the function, yields the corresponding eigenstate's inverse localization length. This criterion, known as "hole closing," is consistent with the GBZ condition in Eq. (6). The Ronkin function can similarly be defined in higher-dimensional systems. Hence, the Amoeba formulation provides a way to generalize non-Bloch band theory to higher-dimensional systems.

III. GENERALIZED SZEGŐ'S LIMIT THEOREM FOR TWO-BAND AII[†] SYSTEMS

In this section, we focus on one-dimensional two-band class AII[†] systems and discuss the limitations of the conventional Amoeba formalism. We introduce band-resolved Ronkin functions that decompose contributions from multiple bands into their respective individual bands. We then demonstrate how band-resolved Ronkin functions can be optimized by extrapolating the total Ronkin function under symmetry constraints. This approach leads to a modified version of the generalized Szegő's limit theorem.

A. Non-Bloch band theory for class-AII[†] systems

Systems in class AII[†] are characterized by the following \mathbb{Z}_2 topological invariant [13]:

$$\begin{aligned} (-1)^{\nu(E)} &= \text{sgn} \left[\frac{\text{Pf}[(E - h_B(\pi))T]}{\text{Pf}[(E - h_B(0))T]} \right] \\ &\times \exp \left\{ -\frac{1}{2} \int_0^\pi dk \partial_k \ln \det[(E - h_B(k))T] \right\}. \end{aligned} \quad (18)$$

The sign function, $\text{sgn}(x)$, takes the value 1 for $x > 0$ and -1 for $x < 0$, and $\text{Pf}[A]$ corresponds to the Pfaffian

of the skew-symmetric matrix A . T is a unitary operator fulfilling TRS^\dagger symmetry defined as

$$T^{-1}h_{\text{B}}(k)T = h_{\text{B}}(-k)^\top, TT^* = -1. \quad (19)$$

When expressed in terms of the non-Bloch Hamiltonian, this symmetry takes the form:

$$T^{-1}h_{\text{nB}}(\beta)T = h_{\text{nB}}(\beta^{-1})^\top. \quad (20)$$

Consequently, the characteristic polynomial remains invariant under the transformation $\beta \rightarrow \beta^{-1}$:

$$\text{ChP}(\beta, E) = \text{ChP}(\beta^{-1}, E). \quad (21)$$

This symmetry ensures that for each root $\beta(E)$, there exist its conjugate root $\beta^{-1}(E)$. Furthermore, the roots can be ordered as,

$$|\beta_{2p}^{-1}| \leq \dots \leq |\beta_1^{-1}| < 1 < |\beta_1| \leq \dots \leq |\beta_{2p}|, \quad (22)$$

resulting in a modified GBZ condition [30]:

$$\text{GBZ}_\sigma = \{\beta \in \mathbb{C}; |\beta_1 \circ E_\sigma(\beta)| = |\beta_{2p} \circ E_\sigma(\beta)|\}. \quad (23)$$

These mathematical properties reflect the existence of Kramers pairs in the spectrum.

B. Breakdown of the Amoeba formulation and band-resolved Ronkin function

The symmetry properties of class-AIII † systems necessitate a modification of the conventional Amoeba formulation in Eq. (12).

Since the Ronkin function becomes even [59], $\mu^* = 0$ always minimizes the Ronkin function. This seemingly implies that all bulk modes are delocalized, and the NHSE is absent in class-AIII † systems. However, this conclusion contradicts both theoretical analyses and numerical results, which consistently demonstrate the existence of localized bulk modes and the NHSE in such systems [13, 30, 59].

For class AIII † systems, we can calculate the Ronkin function in Eq. (13) as

$$R_E(\mu) = \ln |C_E| - 2p\mu + \sum_{j=1}^{2p} (\mu + \mu_j) \cdot \theta(\mu + \mu_j) + \sum_{j=1}^{2p} (\mu - \mu_j) \cdot \theta(\mu - \mu_j), \quad (24)$$

where $\mu_j = \ln |\beta_j(E)|$. Note that all μ_j are positive as required by Eq. (22). By combining Eq. (24) with the GBZ condition Eq. (23), we find that when E lies within the spectrum, regions where the derivative of the Ronkin function equals ± 1 disappear. This observation indicates that μ^* must be explicitly determined by these regions.

However, merely replacing μ^* in Eq. (12) with the value determined by the jump of the derivative from -2

to 0 and the jump from 0 to $+2$, proves insufficient for accurately representing the true potential. The source of this inaccuracy lies in the fact that the Ronkin function integrates contributions from both bands of the system:

$$R_E(\mu) = \sum_{\sigma=+,-} \oint_{\ln |\beta|=\mu} \frac{d\beta}{2\pi i \beta} \ln |E - E_\sigma(\beta)|. \quad (25)$$

Since this μ^* does not simultaneously minimize both bands, the obtained value for the potential differs from the true potential that would correctly include the contributions of both bands at their respective minima.

To address this issue, we can define band-resolved Ronkin functions for each band separately as

$$R_E^{(\sigma)}(\mu) = \oint_{\ln |\beta|=\mu} \frac{d\beta}{2\pi i \beta} \ln |E - E_\sigma(\beta)|. \quad (26)$$

We can expect that optimizing each function yields appropriate values for the potentials $\Phi_\sigma(E)$ and localization lengths μ_σ for each band.

This approach would seemingly resolve the optimization problems described above. However, this straightforward definition of band-resolved Ronkin functions proves challenging. The problem arises from the following critical issues: These band-resolved Ronkin functions exhibit an explicit dependence on the branch cuts of the EBB. Although Eq. (26) can be used to calculate band-resolved Ronkin functions, it remains unclear which energy corresponds to each band-wise Ronkin function. Simply using the eigenvalues of $h_{\text{nB}}(\beta)$ results in a loss of essential mathematical properties. The resulting band-resolved Ronkin functions are neither convex nor piecewise linear, as demonstrated in Appendix A.

These limitations necessitate an alternative approach to defining band-resolved Ronkin functions. The following section presents a modified formulation that preserves the crucial mathematical properties while adequately accounting for the band structure.

C. Constructing band-resolved Ronkin functions

Szegő's limit theorem, Eq. (10), holds when $\nu(E)$ is trivial. Therefore, we focus here on the case where $\nu(E)$ is topologically nontrivial.

First, we outline the mathematical properties that the band-resolved Ronkin function $R_E^{(\pm)}$ must have. The band-resolved Ronkin functions should inherit the mathematical properties of the total Ronkin function R_E : they must be convex, piece-wise linear, and have integer-quantized derivatives. Furthermore, we require that $R_E^{(\pm)}$ exhibit hole closing if E is in the OBC spectrum, analogous to the class A case. Considering Eq. (23), we assume that $R_E^{(+)}[R_E^{(-)}]$ remains constant in the domain $\mu_1 \leq \mu \leq \mu_2$ [$-\mu_2 \leq \mu \leq -\mu_1$].

Next, we discuss how the TRS^\dagger constrains the band resolved functions. When a system satisfies TRS^\dagger ,

each state is doubly degenerate, forming Kramers pairs, and the states in each pair exhibit opposite localization lengths. Consequently, we require the band-resolved Ronkin functions to have the same optimal value and to satisfy the following relation:

$$R_E(\mu) = R_E^{(+)}(\mu) + R_E^{(-)}(\mu), \quad R_E^{(+)}(\mu) = R_E^{(-)}(-\mu). \quad (27)$$

To construct such proper band-resolved Ronkin functions, we use Eq. (24), which shows that the total Ronkin function is determined by the β -roots and the poles enclosed by the circle $|\beta| = e^\mu$. Therefore, we divide the roots and the order of the pole into two groups. We assume that $R_E^{(+)} [R_E^{(-)}]$ contains the roots whose moduli are larger [smaller] than 1. From the above assumption, we can deduce that the $R_E^{(+)} [R_E^{(-)}]$ must remain constant in the domain $\mu_1 \leq \mu \leq \mu_2 [-\mu_2 \leq \mu \leq -\mu_1]$. Thus, the order of poles must be divided into 1 and $2p - 1$.

Accordingly, the band-resolved Ronkin functions are given by,

$$\begin{aligned} R_E^{(+)}(\mu) &= \frac{1}{2} \ln |C_E| - \frac{1}{2} \sum_{j=1}^{2p} \mu_j - \mu \\ &\quad + \sum_{j=1}^{2p} (\mu - \mu_j) \cdot \theta(\mu - \mu_j), \\ R_E^{(-)}(\mu) &= \frac{1}{2} \ln |C_E| + \frac{1}{2} \sum_{j=1}^{2p} \mu_j - (2p - 1)\mu \\ &\quad + \sum_{j=1}^{2p} (\mu + \mu_j) \cdot \theta(\mu + \mu_j) \end{aligned} \quad (28)$$

Here, the second term provides a constant shift, ensuring that the band-resolved Ronkin functions satisfy Eq. (27). The band-resolved Ronkin functions introduced here maintain the symmetry between bands while preserving the piecewise linearity and integer-valued derivatives of the Ronkin functions. One can readily verify that the sum of these band-resolved Ronkin functions reproduces the total Ronkin function in Eq. (24).

D. Reconstruction of the total Ronkin function and generalized Szegő's limit theorem

We reconstruct the total Ronkin function using this decomposition and demonstrate that the extrapolation of the total Ronkin function optimizes the band-resolved Ronkin functions, leading to a generalized Szegő's limit theorem for two-band class AIII systems.

The band-resolved Ronkin functions defined in

Eq. (28) can be expanded around their minima as

$$R_E^{(+)}(\mu) = a + \begin{cases} -(\mu - \mu_1) & -\infty \leq \mu \leq \mu_1 \\ 0 & \mu_1 \leq \mu \leq \mu_2 \\ \mu - \mu_2 & \mu_2 \leq \mu \leq \mu_3 \end{cases} \quad (29)$$

$$R_E^{(-)}(\mu) = a + \begin{cases} -(\mu + \mu_2) & -\mu_3 \leq \mu \leq -\mu_2 \\ 0 & -\mu_2 \leq \mu \leq -\mu_1 \\ \mu + \mu_1 & -\mu_1 \leq \mu \leq \infty \end{cases} \quad (30)$$

Here a denotes the minimum of the band-resolved Ronkin functions,

$$a = \frac{1}{2} \ln |C_E| - \frac{1}{2} \mu_1 + \frac{1}{2} \sum_{j=2}^{2p} \mu_j, \quad (31)$$

which corresponds to the potential of each band.

Because the total Ronkin function is symmetric, we focus on $\mu \geq 0$ and can easily reconstruct the total Ronkin function as

$$R_E(\mu) = 2a + \begin{cases} 2\mu_1 & 0 \leq \mu \leq \mu_1 \\ \mu + \mu_1 & \mu_1 \leq \mu \leq \mu_2 \\ 2\mu - (\mu_2 - \mu_1) & \mu_2 \leq \mu \leq \mu_3 \end{cases} \quad (32)$$

We observe that the minimum of the Ronkin function is shifted by $2\mu_1$ from the optimal value $2a$. Therefore, we can obtain the true potential by correcting this error. However, merely correcting this shift would result in the loss of hole-closing information, which plays a crucial role in the spectral detection for class A systems. Thus, we focus on $\mu_2 - \mu_1$, which represents the length of the region with a slope of 1, as this region vanishes when E belongs to the OBC spectrum.

With this knowledge, we can now extrapolate the full Ronkin function to obtain the correct potential. By extrapolating the region with a slope of 2, we obtain the

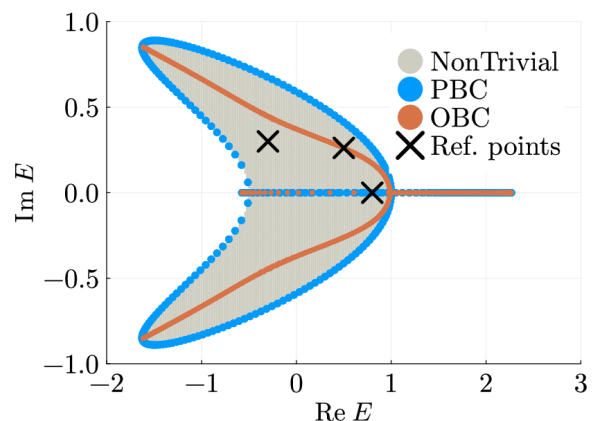


FIG. 1: PBC and OBC ($N = 400$) spectrum: The Hamiltonian is defined in Eq. (37). Parameters are set to $t_1 = 0.3, t_2 = 0.8, g_{1,x} = 0.3, g_{1,z} = 0.5i, g_{2,x} = 0.2$. The topologically nontrivial area is filled in gray. The reference points are $E = -0.3 + 0.3i, 0.5 + 0.265i, 0.8$.

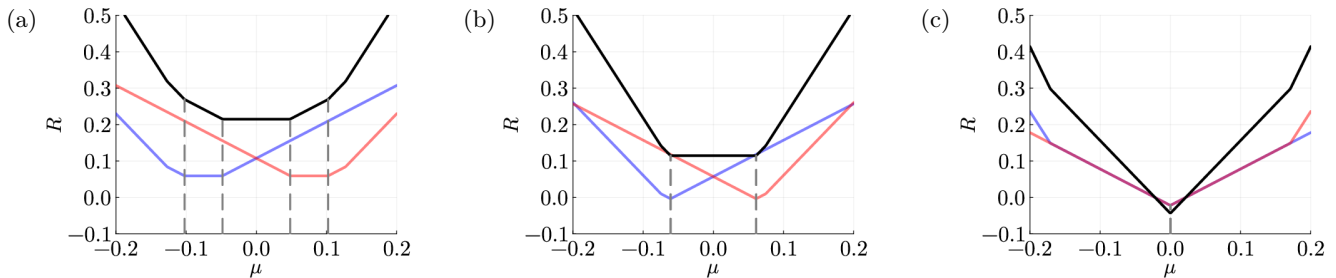


FIG. 2: Band-resolved Ronkin functions for (a) $E = -0.3 + 0.3i$, (b) $E = 0.5 + 0.265i$, and (c) $E = 0.8$: The Hamiltonian and parameters are identical to those in Fig. 1. The red, blue and black lines represent $R_E^{(+)}$, $R_E^{(-)}$ and R_E , respectively. The black dashed lines indicate the region with slope ± 1 . The total Ronkin function is symmetric, and the band-resolved Ronkin functions $R^{(\pm)}$ satisfy the symmetry relation in Eq. (27). For points not inside the OBC spectrum [(a)], the regions with slope ± 1 remain. For points inside the OBC spectrum [(b) and (c)], the regions with slope ± 1 of the total Ronkin function vanish, which corresponds to the hole closing in the band-resolved Ronkin functions.

correct potential:

$$\Phi(E) = \tilde{R}_E^{(2)}(0) + (\mu_2 - \mu_1), \quad (33)$$

where $\tilde{R}_E^{(2)}(\mu) = 2\mu + 2a - (\mu_2 - \mu_1)$. Combining the GBZ condition Eq. (23), the extrapolated value yields the appropriate potential for the OBC spectrum, and the localization length is obtained by $\mu_1 (= \mu_2)$.

Notably, this extrapolation method works even when the region with a slope of 2 vanishes. If $\mu_2 = \mu_3$ holds, we can consider the tangent line with a slope of 2 at $\mu = \mu_2$. This condition motivates us to reformulate Eq. (33) in terms of the Legendre transformation.

We introduce the Legendre transformation of the Ronkin function, which takes the form

$$Q_E(m) = \min_{\mu} [R_E(\mu) - m\mu]. \quad (34)$$

In this framework, we can define the correct potential of the generalized Szegő's limit theorem for two-band class AIII † systems using

$$\Phi(E) = Q_E(2) - (Q'_E(1 + \epsilon) - Q'_E(1 - \epsilon)) \quad (35)$$

where Q'_E denotes the derivative of Q_E , and ϵ represents an infinitesimal positive parameter [65].

We can finally include the trivial case and summarize our conjecture to compute the OBC potential Eq. (9) as

$$\Phi(E) = \begin{cases} Q_E(0) & \nu(E) = 0 \\ Q_E(2) - (Q'_E(1 + \epsilon) - Q'_E(1 - \epsilon)) & \nu(E) = 1 \end{cases}. \quad (36)$$

The information about hole closing is inherited as the jump in the derivative Q'_E at $m = 1$. Thus, the absence of such a jump serves as an indicator of the OBC spectrum.

IV. NUMERICAL VERIFICATION

Finally, in this section, we numerically demonstrate the correctness of our assumptions by calculating the potential and DOS using Eq. (36).

We use the following Bloch Hamiltonian in class AIII † ,

$$h_B(k) = [2t_1 \cos k + 2t_2 \cos 2k]\sigma_0 - [2g_1 \sin k + 2g_2 \sin 2k] \cdot \boldsymbol{\sigma} \quad (37)$$

where σ_0 is the unit matrix, and $\sigma_{x,y,z}$ are the Pauli matrices. The operator T defined in Eq. (19) is given by σ_y . The Hamiltonian can be diagonalized straightforwardly as,

$$E_{\pm}(k) = 2t_1 \cos k + 2t_2 \cos 2k \pm 2\|g_1 \sin k + g_2 \sin 2k\|. \quad (38)$$

We set the parameters as $t_1 = 0.3, t_2 = 0.8, g_1 = (0.3, 0.0, 0.5i), g_2 = (0.2, 0.0, 0.0)$.

Figure 1 shows the spectrum obtained by diagonalizing the finite-size Hamiltonian on a chain with 400 sites. The blue and orange lines represent the spectra under PBC and OBC, respectively. The complex plane contains a region with a nontrivial \mathbb{Z}_2 topological invariant, as defined in Eq. (18) (shaded in gray). The OBC spectrum coincides with the PBC spectrum along the real axis. Both spectra match for $\text{Re } E > 1$ but differ for $\text{Re } E < 1$. While the PBC spectrum is gapless, the OBC spectrum appears to exhibit a line gap at $E = 0.8$. However, this gap arises due to finite-size effects and vanishes in the thermodynamic limit.

We show the total Ronkin functions and the band-resolved Ronkin functions in Fig. 2. The reference points are set as $-0.3 + 0.3i$ [(a)], $E = 0.5 + 0.265i$ [(b)], and 0.8 [(c)]. In each figure, the red, blue, and black lines represent $R_E^{(+)}$, $R_E^{(-)}$ and R_E , respectively. Due to TRS † constraints, the total Ronkin function is symmetric around $\mu = 0$. The band-resolved Ronkin functions $R^{(\pm)}$

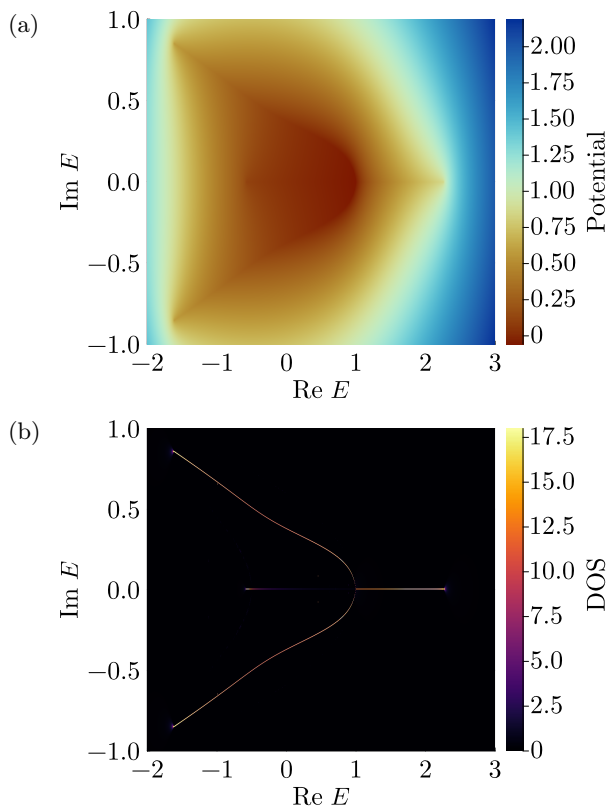


FIG. 3: Spectral potential (a) and DOS given by this potential using Eq. (8) in (b): The Hamiltonian and parameters are identical to those in Fig. 1. The direct diagonalization shows a ψ -shaped spectral distribution [Fig. (1)], which is successfully reproduced by our conjecture proposed in Eq. (36).

inherit the mathematical properties of the total function, i.e., they are convex, piece-wise linear, and have integer-quantized derivatives. Furthermore, they satisfy the symmetry relation in Eq. (27). For points outside the OBC spectrum [Fig. 2(a)], the regions with slope ± 1 , indicated by black dashed lines, remain. For points inside the OBC spectrum [Fig. 2(b), (c)], the regions with slope ± 1 in the total Ronkin function vanish, which corresponds to the hole closing in the band-resolved Ronkin functions. These results are consistent with the GBZ condition in Eq. (23).

Figure 3 shows the potential and the DOS using Eq. (36). Our modified Amoeba formulation works in topologically nontrivial domains and successfully predicts the ψ -shaped spectral distribution, consistent with numerical diagonalization results [Fig. 1].

Finally, to examine the generalized Szegő's limit theorem, we perform finite-size analysis and calculate the maximum difference between the exact potential $\phi(E)$ (calculated by Eq. (9)) and our proposed potential $\Phi(E)$ using Eq. (33), shown in Fig. 4. The difference converges to zero in the thermodynamic limit ($N \rightarrow \infty$) with scaling $\mathcal{O}(N^{-1})$, which shows the validity of our conjecture.

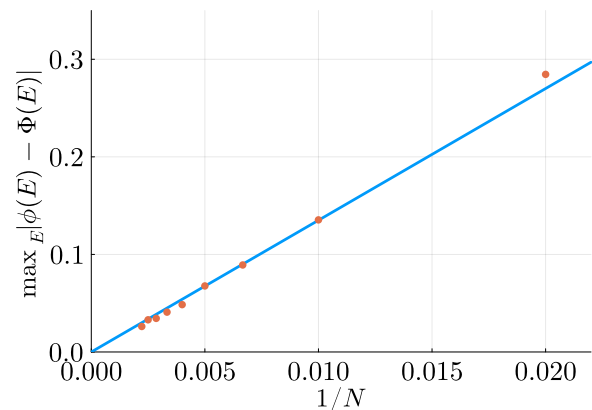


FIG. 4: The maximum difference, $\max_E |\phi(E) - \Phi(E)|$, between the OBC potential and the potential calculated by the Ronkin function for various system sizes $N = 50, 100, \dots, 450$. The Hamiltonian and parameters are identical to those in Fig. 1. The difference converges to zero in the limit $N \rightarrow \infty$ with scaling $\mathcal{O}(N^{-1})$.

V. CONCLUSIONS

The Amoeba formulation has opened a new path for studying the GBZ in higher dimensions. However, the multiband nature and symmetry-protected degeneracies invalidate the conventional Amoeba formulation since the optimization problem becomes invalid.

This paper partially solves this problem, focusing on one-dimensional two-band class AII † systems. Due to symmetry constraints based on TRS † , we can decompose the Ronkin functions into band-resolved functions and reconstruct the generalized Szegő's limit theorem, which can be calculated using the Legendre transformation. We finally numerically demonstrate the correctness of our conjectures by calculating the spectrum of a two-band class AII † system and showing the validness of the modified Szegő's limit by comparing with exact diagonalization.

We note that a generalization of this extrapolation method to higher-dimensional cases remains challenging. In one-dimensional systems, both the total Ronkin function and band-resolved Ronkin functions are piecewise linear, which helps recover the correct potential. However, the Ronkin function is no longer linear in higher-dimensional systems, making the extrapolation problematic.

ACKNOWLEDGMENTS

S.K. deeply appreciates the fruitful discussions with D. Nakamura, K. Shimomura, and K. Shinada. This work is supported by JSPS, KAKENHI Grants No. JP24KJ1353 (S.K.), and No. JP23K03300 (R.P.).

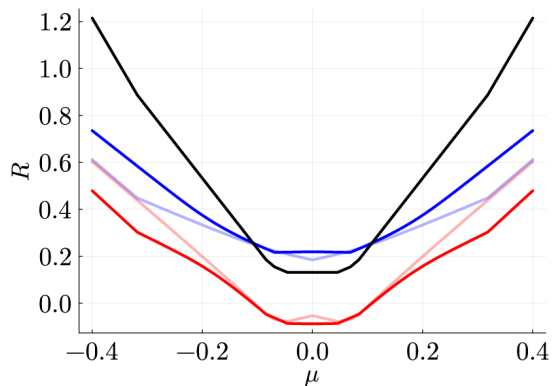


FIG. 5: Band-resolved Ronkin functions via EBB and the total function for $E = 0.5 + 0.3i$ with parameters identical from Fig. 1: Branch cuts of the square root extend from the origin at angles of $5\pi/7$ (red/blue) and 0 (light red/light blue). While their sum yields the total Ronkin function (black line), these band-resolved functions are neither convex nor integer-quantized derivatives.

APPENDIX

A. Band-resolved Ronkin functions using the energy branch branches

In this appendix, we demonstrate that the band-resolved Ronkin functions defined with the EBB [Eq. (26)] break convexity and are not piece-wise linear.

We calculate the band-resolved Ronkin functions with the EBBs defined in Eq. (38). Parameters are set as in Fig. 1. We plot the total and the band-resolved Ronkin functions for $E = 0.5 + 0.3i$ in Fig. 5. The red and blue lines represent $R_E^{(+)}$ and $R_E^{(-)}$, respectively, while

the black line shows the total function R_E . The EBBs include the square root of a complex number and, thus, depend on the branch cut. We here consider two choices of branch cuts for the square root: a half line from the origin to infinity at angles of $5\pi/7$ (red and blue) and 0 (light red and light blue). The partial functions $R_E^{(+)}$ and $R_E^{(-)}$ have different minimal values, and their shapes strongly depend on the choice of branch cuts. Furthermore, the optimal value μ^* varies with different branch cut configurations. Although the sum of the band-resolved Ronkin functions yields R_E for both branch cut choices, they violate convexity and lack integer-quantized derivatives.

While we can expect that a well-designed branch cut recovers the mathematical properties of the partial functions, there are some cases where this is impossible. The absence of convexity and integer-quantized derivatives arises from the fact that the EBBs $E_\sigma(\beta)$ are algebraic functions rather than Laurent polynomials. If an EBB is a Laurent polynomial, the function is analytical over the complex plane except the origin. Consequently, the contour along the circle $|\beta| = e^\mu$ forms a closed curve. Since the derivatives of the band-resolved Ronkin function count the winding number of this curve around E [58], this closed curve induces the aforementioned mathematical characteristics. However, if the EBB is an algebraic function, it can have additional singularities, causing each branch to form arcs rather than a closed curve. Such an arc structure results in non-integer winding numbers, thereby breaking the quantization of the derivatives. Changing the branch cut is equivalent to cutting and reconnecting these arcs. Thus, we can reconstruct a closed curve for a single EBB using a well-designed branch cut. However, when several arcs form a single closed curve, called braiding, such a reconfiguration by choosing branch cuts becomes impossible.

-
- [1] Y. Ashida, Z. Gong, and M. Ueda, Non-hermitian physics, *Adv. Phys.* **69**, 249 (2020).
 - [2] E. J. Bergholtz, J. C. Budich, and F. K. Kunst, Exceptional topology of non-hermitian systems, *Rev. Mod. Phys.* **93**, 015005 (2021).
 - [3] K. Ding, C. Fang, and G. Ma, Non-hermitian topology and exceptional-point geometries, *Nature Reviews Physics* **4**, 745 (2022-12).
 - [4] S. Yao and Z. Wang, Edge states and topological invariants of non-hermitian systems, *Phys. Rev. Lett.* **121**, 086803 (2018).
 - [5] F. K. Kunst, E. Edvardsson, J. C. Budich, and E. J. Bergholtz, Biorthogonal bulk-boundary correspondence in non-hermitian systems, *Phys. Rev. Lett.* **121**, 026808 (2018).
 - [6] K. Yokomizo and S. Murakami, Non-bloch band theory of non-hermitian systems, *Phys. Rev. Lett.* **123**, 066404 (2019).
 - [7] Z. Yang, K. Zhang, C. Fang, and J. Hu, Non-hermitian bulk-boundary correspondence and auxiliary generalized brillouin zone theory, *Phys. Rev. Lett.* **125**, 226402 (2019), [arXiv:cond-mat/1905.08111](https://arxiv.org/abs/cond-mat/1905.08111).
 - [8] K. Kawabata, K. Shiozaki, M. Ueda, and M. Sato, Symmetry and topology in non-hermitian physics, *Phys. Rev. X* **9**, 041015 (2019).
 - [9] C. H. Lee and R. Thomale, Anatomy of skin modes and topology in non-hermitian systems, *Phys. Rev. B* **99**, 201103 (2019).
 - [10] F. K. Kunst and V. Dwivedi, Non-hermitian systems and topology: A transfer-matrix perspective, *Phys. Rev. B* **99**, 245116 (2019).
 - [11] F. Song, S. Yao, and Z. Wang, Non-hermitian topological invariants in real space, *Phys. Rev. Lett.* **123**, 246801 (2019).
 - [12] K. Zhang, Z. Yang, and C. Fang, Correspondence between winding numbers and skin modes in non-hermitian systems, *Phys. Rev. Lett.* **125**, 126402 (2020).
 - [13] N. Okuma, K. Kawabata, K. Shiozaki, and M. Sato,

- Topological origin of non-hermitian skin effects, *Phys. Rev. Lett.* **124**, 086801 (2020).
- [14] L. Li, C. H. Lee, S. Mu, and J. Gong, Critical non-hermitian skin effect, *Nat. Commun.* **11**, 5491 (2020-12).
- [15] K. Kawabata, M. Sato, and K. Shiozaki, Higher-order non-hermitian skin effect, *Phys. Rev. B.* **102**, 205118 (2020).
- [16] S. Longhi, Non-bloch-band collapse and chiral zener tunneling, *Phys. Rev. Lett.* **124**, 066602 (2020).
- [17] Y. Yi and Z. Yang, Non-hermitian skin modes induced by on-site dissipations and chiral tunneling effect, *Phys. Rev. Lett.* **125**, 186802 (2020).
- [18] K. Yokomizo and S. Murakami, Scaling rule for the critical non-hermitian skin effect, *Phys. Rev. B.* **104**, 165117 (2021).
- [19] R. Okugawa, R. Takahashi, and K. Yokomizo, Non-hermitian band topology with generalized inversion symmetry, *Phys. Rev. B.* **103**, 205205 (2021).
- [20] M. Lu, X.-X. Zhang, and M. Franz, Magnetic suppression of non-hermitian skin effects, *Phys. Rev. Lett.* **127**, 256402 (2021).
- [21] D. Wu, J. Xie, Y. Zhou, and J. An, Connections between the open-boundary spectrum and the generalized brillouin zone in non-hermitian systems, *Phys. Rev. B.* **105**, 045422 (2022).
- [22] Q. Liang, D. Xie, Z. Dong, H. Li, H. Li, B. Gadway, W. Yi, and B. Yan, Dynamic signatures of non-hermitian skin effect and topology in ultracold atoms, *Phys. Rev. Lett.* **129**, 070401 (2022).
- [23] F. Song, H.-Y. Wang, and Z. Wang, Non-bloch PT symmetry: Universal threshold and dimensional surprise, in *A Festschrift in Honor of the C N Yang Centenary* (WORLD SCIENTIFIC, 2022) pp. 299–311.
- [24] S. Longhi, Non-hermitian skin effect and self-acceleration, *Phys. Rev. B.* **105**, 245143 (2022).
- [25] Z. Gu, H. Gao, H. Xue, J. Li, Z. Su, and J. Zhu, Transient non-hermitian skin effect, *Nat. Commun.* **13**, 7668 (2022).
- [26] K. Kawabata, T. Numasawa, and S. Ryu, Entanglement phase transition induced by the non-hermitian skin effect, *Phys. Rev. X.* **13**, 021007 (2023).
- [27] C.-A. Li, B. Trauzettel, T. Neupert, and S.-B. Zhang, Enhancement of second-order non-hermitian skin effect by magnetic fields, *Phys. Rev. Lett.* **131**, 116601 (2023).
- [28] K. Zhang, Z. Yang, and K. Sun, Edge theory of non-hermitian skin modes in higher dimensions, *Phys. Rev. B.* **109**, 165127 (2024).
- [29] Y.-L. Zhang, L.-W. Wang, Y. Liu, Z.-X. Chen, and J.-H. Jiang, Hybrid skin-topological effect in non-hermitian checkerboard lattices with large chern numbers (2024), [arXiv:2411.07465](https://arxiv.org/abs/2411.07465).
- [30] K. Kawabata, N. Okuma, and M. Sato, Non-bloch band theory of non-hermitian hamiltonians in the symplectic class, *Phys. Rev. B.* **101**, 195147 (2020).
- [31] H. Hu and E. Zhao, Knots and non-hermitian bloch bands, *Phys. Rev. Lett.* **126**, 010401 (2021).
- [32] K. Yokomizo and S. Murakami, Non-bloch band theory in bosonic bogoliubov-de gennes systems, *Phys. Rev. B.* **103**, 165123 (2021).
- [33] T. Li, J.-Z. Sun, Y.-S. Zhang, and W. Yi, Non-bloch quench dynamics, *Phys. Rev. Res.* **3**, 023022 (2021).
- [34] G.-F. Guo, X.-X. Bao, and L. Tan, Non-hermitian bulk-boundary correspondence and singular behaviors of generalized brillouin zone, *New J. Phys.* **23**, 123007 (2021-02).
- [35] W.-T. Xue, M.-R. Li, Y.-M. Hu, F. Song, and Z. Wang, Simple formulas of directional amplification from non-bloch band theory, *Phys. Rev. B.* **103**, L241408 (2021).
- [36] Y. Li, X. Ji, Y. Chen, X. Yan, and X. Yang, Topological energy braiding of non-bloch bands, *Phys. Rev. B.* **106**, 195425 (2022).
- [37] H. Li and S. Wan, Exact formulas of the end-to-end green's functions in non-hermitian systems, *Phys. Rev. B.* **105**, 045122 (2022).
- [38] Y.-M. Hu and Z. Wang, Green's functions of multiband non-hermitian systems, *Phys. Rev. Res.* **10.48550/arXiv.2304.14438** (2023).
- [39] Y.-M. Hu, Y.-Q. Huang, W.-T. Xue, and Z. Wang, Non-bloch band theory for non-hermitian continuum systems, *Phys. Rev. B.* **10.48550/arXiv.2310.08572** (2023), [arXiv:cond-mat.mes-hall](https://arxiv.org/abs/2310.08572).
- [40] H. Liu, M. Lu, Z.-Q. Zhang, and H. Jiang, Modified generalized brillouin zone theory with on-site disorder, *Phys. Rev. B.* **107**, 144204 (2023).
- [41] T. Tai and C. H. Lee, Zoology of non-hermitian spectra and their graph topology, *Phys. Rev. B.* **107**, L220301 (2023).
- [42] K. Matsushima and T. Yamada, Non-bloch band theory for time-modulated discrete mechanical systems (2024), [arXiv:2407.09871](https://arxiv.org/abs/2407.09871).
- [43] S. Verma and M. J. Park, Non-bloch band theory of sub-symmetry-protected topological phases (2024), [arXiv:2405.06240](https://arxiv.org/abs/2405.06240).
- [44] H.-R. Wang, Z. Wang, and Z. Wang, Non-bloch self-energy of dissipative interacting fermions (2024), [arXiv:2411.13661](https://arxiv.org/abs/2411.13661).
- [45] K. Roy, K. Gogoi, and S. Basu, Topological characterization of a non-hermitian ladder via floquet non-bloch theory (2024), [arXiv:2410.05427](https://arxiv.org/abs/2410.05427).
- [46] Z. Yang, C. Lu, and X. Lu, Entanglement entropy on generalized brillouin zone, *Phys. Rev. B.* (2024).
- [47] Y. Fu and Y. Zhang, Braiding topology of non-hermitian open-boundary bands, *Phys. Rev. B.* (2024), [arXiv:cond-mat.mes-hall](https://arxiv.org/abs/cond-mat.mes-hall).
- [48] Z. Yang, C. Lu, and X. Lu, Entanglement entropy on generalized brillouin zone, *Phys. Rev. B.* **10.48550/arXiv.2406.15564** (2024).
- [49] S.-X. Wang and Z. Yan, General theory for infernal points in non-hermitian systems, *Phys. Rev. B.* **110**, L201104 (2024).
- [50] Y.-M. Hu, H.-Y. Wang, Z. Wang, and F. Song, Geometric origin of non-bloch P T symmetry breaking, *Phys. Rev. Lett.* **132**, 050402 (2024).
- [51] Q. Li, H. Jiang, and C. H. Lee, Phase-space generalized brillouin zone for spatially inhomogeneous non-hermitian systems, [arXiv:2501.09785](https://arxiv.org/abs/2501.09785).
- [52] S. Yao, F. Song, and Z. Wang, Non-hermitian chern bands, *Phys. Rev. Lett.* **121**, 136802 (2018).
- [53] T. Liu, Y.-R. Zhang, Q. Ai, Z. Gong, K. Kawabata, M. Ueda, and F. Nori, Second-order topological phases in non-hermitian systems, *Phys. Rev. Lett.* **122**, 076801 (2019).
- [54] K. Yokomizo and S. Murakami, Non-bloch bands in two-dimensional non-hermitian systems, *Phys. Rev. B.* **107**, 195112 (2023).
- [55] H. Jiang and C. H. Lee, Dimensional transmutation from non-hermiticity, *Phys. Rev. Lett.* **131**, 076401 (2023).
- [56] Z. Xu, B. Pang, K. Zhang, and Z. Yang, Two-dimensional

- asymptotic generalized brillouin zone conjecture (2023), arXiv:2311.16868.
- [57] K. Zhang, C. Shu, and K. Sun, [Algebraic non-hermitian skin effect and unified non-bloch band theory in arbitrary dimensions](#) (2024), arXiv:2406.06682.
- [58] H.-Y. Wang, F. Song, and Z. Wang, Amoeba formulation of non-bloch band theory in arbitrary dimensions, [Phys. Rev. X](#) **14**, 021011 (2024).
- [59] S.-X. Wang, Constraints of internal symmetry on the non-hermitian skin effect and bidirectional skin effect under the action of the hermitian conjugate of time-reversal symmetry, [Phys. Rev. B](#) **109**, L081108 (2024).
- [60] Y. Xiong and H. Hu, [Graph morphology of non-hermitian bands](#) (2023), arXiv:2311.14921.
- [61] Y. Xiong, Z.-Y. Xing, and H. Hu, [Non-hermitian skin effect in arbitrary dimensions: non-bloch band theory and classification](#) (2024), arXiv:2407.01296.
- [62] H. Hu, Topological origin of non-hermitian skin effect in higher dimensions and uniform spectra, [Sci. Bull. \(Beijing\)](#) **70**, 51 (2025).
- [63] Y. Fu and Y. Zhang, Anatomy of open-boundary bulk in multiband non-hermitian systems, [Phys. Rev. B](#) **107**, 115412 (2023).
- [64] G. Szegő, Ein grenzwertsatz über die toeplitzischen determinanten einer reellen positiven funktion, [Math. Ann.](#) **76**, 490 (1915).
- [65] Since the Ronkin function is piecewise linear and has integer-quantized derivatives, the following equivalent expression exists: $\Phi(E) = Q_E(2) - (Q'_E(2 - \epsilon) - Q'_E(0 + \epsilon))$.